This article has been published in Biomaterials and Biosystems. The final publication is available from Elsevier at https://doi.org/10.1016/j.bbiosy.2021.100013.

Current interpretations on the *in vivo* response of bone to additively manufactured metallic porous scaffolds: a review

Joseph Deering[1], Kathryn Grandfield[1,2*]

[1] Department of Materials Science and Engineering, McMaster University, Hamilton, ON, Canada

[2] School of Biomedical Engineering, McMaster University, Hamilton, ON, Canada

[*] Corresponding author:

Prof. Kathryn Grandfield
McMaster University
1280 Main Street West
Hamilton, ON, L8S 4L7
Canada
Email: kgrandfield@mcmaster.ca
Phone: +1 905.525.9140 Ext. 23573

1 Abstract

Recent advances in the field of metallic additive manufacturing have expanded production capabilities for bone implants to include porous lattice structures. While traditional models of *de novo* bone formation can be applied to fully dense implant materials, their applicability to the interior of porous materials has not been well-characterized. Unlike other reviews that focus on materials and mechanical properties of lattice structures, this review compiles biological performance from *in vivo* studies in pre-clinical models only. First, we introduce the most common lattice geometry designs employed *in vivo* and discuss some of their fabrication advantages and limitations. Then lattice geometry is correlated to quantitative (histomorphometric) and qualitative (histological) assessments of osseointegration. We group studies according to two common implant variables: pore size and percent porosity, and explore the extent of osseointegration using common measures, including bone-implant contact (BIC), bone area (BA), bone volume/total volume (BV/TV) and biomechanical stability, for various animal models and implantation times. Based on this, trends related to *in vivo* bone formation on the interior of lattice structures are presented. Common challenges with lattice structures are highlighted, including nonuniformity of bone growth through the entirety of the lattice structure due to occlusion effects and avascularity. This review paper identifies a lack of systematic *in vivo* studies on porous AM implants to target optimum geometric design, including pore shape, size, and percent porosity in controlled animal

models and critical-sized defects. Further work focusing on surface modification strategies and systematic geometric studies to homogenize *in vivo* bone growth through the scaffold interior are recommended to increase implant stability in the early stages of osseointegration.

Keywords: Osseointegration; additive manufacturing, 3D printing, histomorphometry, metallic implant design; in vivo; porous; tissue engineering

2 Scaffold Design and Fabrication

2.1 Introduction

Metallic additive manufacturing (AM) processes are beginning to see increased usage in the world of bone implants, especially for dental and orthopaedic implants, due to their ability to fabricate complex geometries, particularly porous lattice structures. The ability to produce porous implants presents two main advantages for this field. Firstly, it presents the potential for improvement in osseointegration – a long-term structural and functional connection between bone and implant – enabled by the complex pore system that provides superior mechanical interlocking effects. Early-stage osteoconduction – the process where bone conforms to a surface or biomaterial [1] – depends heavily on the design of the scaffold geometry, including pore size and shape. Secondly, where load-bearing implants may suffer from stress shielding, onset by increased bone resorption rates in the presence of high elastic modulus metallic implants [2], porous metallic structures can lead to an effective stiffness reduction mechanism by intentionally introducing porosity to implant geometries. Generally, reduction in stiffness responds by an exponential or power relationship as porosity increases [3,4] due to a change in the second moment of area [3]. Towards the same effort, novel titanium alloys with high niobium and zirconium content have been developed [5–9] to reduce the elastic moduli of titanium materials by changing the bonding structure and phase stability while maintaining biocompatibility and ease of processing with AM [10]. As the benchmark material for traditional implants, alloys of titanium often have elastic moduli in the range of 55-117 GPa, which can be reduced to the range of cortical bone (3-20 GPa) by intentional introduction of porosity [11]. Conventional biomaterial alloys with high elastic moduli, such as stainless steel or CoCr (both on the order of 200 GPa), can also make use of AM methodologies to create lattice structures to similarly reduce implant stiffness into the range of cortical bone without sacrificing their inherent biocompatibility [12,13].

Previous reviews on the usage and development of porous metallic materials have predominantly focused on broad development of these materials, including materials selection [14,15], design considerations [16–18], surface modification [16,17], and mechanical properties [17], with only superficial investigation of the resulting bone structure from a biological perspective following implant retrieval. In a review from Weber, special consideration has been given to bone formation along porous structures to introduce the importance of design factors in relation to osteogenesis [19]. However, to optimize lattice conditions for bone ingrowth in humans, a comprehensive review of pre-clinical *in vivo* models is first needed to evaluate how these porous implants behave in various animals. In this evaluation, one must consider the effect of the lattice geometry on materials and mechanical properties, the limitations of particular printing methods, and most importantly their corresponding influence on osseointegration and osteoconduction. In the following sections we present a brief summary of printing methods prior to the ultimate focus of

this work: understanding the biological effects of these implant geometries on bone tissue, as summarized using quantitative measures from histomorphometry and qualitative histological observations.

2.2 AM Fabrication Techniques for Porous Metallic Implants Studied In Vivo

Several AM methods exist for the production of porous metallic scaffolds in bone applications. Where comprehensive outlines of each AM process exist in the literature for metal fabrication [20–22], here we briefly describe the relevant scope and limitations for the most common types of AM processes in the production of porous materials.

The most common forms of powder bed processes include selective laser sintering (SLS), selective laser melting (SLM), direct metal laser sintering (DMLS), and electron beam melting (EBM). The minimum size for an SLM part is dependent on factors such as powder absorptivity [23], but the stability of the molten pool has been observed to decrease in stability as the energy density increases [24]. This can result in material ejection from the melt pool [25] and a part that is susceptible to defects [26]. The production of porous materials also requires overhanging components. As the strut angle deviates further from the normal in powder bed processes, there is a marked decrease in geometric accuracy of the part [27]. An investigation of this phenomenon in EBM and SLM materials has shown that deviations up to 10% can occur and that this effect is more pronounced in EBM materials [28]. These factors along with the commercial availability of powders and energy source optics mean that the minimum size of stable struts in a porous material is restricted to roughly 200 μm.

Directed energy deposition alternatives to powder bed methods include laser engineered net shaping (LENS®), direct metal deposition (DMD), and laser metal deposition. Analysis of LENS parts has shown substantial residual stresses that can accumulate due to their thermal history [29,30]. Without further post-processing, these stresses can cause complications including premature part failure. Directed energy deposition methods are also classified to have lower resolution, low-quality surface finishes, and the inability to produce complex geometries compared to powder bed processes [31]. The lower accuracy of DED processes further restricts the minimum strut size and accessible geometries compared to what is available in powder bed techniques. Of the papers surveyed in this review, nearly 98% of porous implants for in vivo studies were produced by powder-bed techniques (78% SLM, 12% EBM, 5% SLS, 3% DMLS), while only 2% were produced by DED or laser engineered net shaping. The dominant reason for this likely pertains to ease of manufacturing and equipment abundance rather than *in vivo* response.

Most porous metallic structures for in vivo implantation focus on traditional implant materials. Commercially pure titanium and Ti-6Al-4V have extensively been used in the literature for animal studies due to their well-defined processing parameters in SLM, but novel biocompatible alloys containing niobium, tantalum and zirconium are also being developed [32–35]. The addition of β-stabilizing elements in titanium should mitigate some stress-shielding effects [36] to further modify a porous structure's osseointegration potential. Many of these novel alloys have not yet been implemented in porous structures for testing in pre-clinical trials. Almost all of the AM implant materials studied *in vivo* in this review were commercially pure titanium (44%) or Ti-6Al-4V (53%), with materials such as tantalum or iron-manganese composing the remaining 3%. Other

materials including NiTi [37,38], polyamide [39], and stainless steel [40] have been used for porous implants, but not using metallic AM.

Another common observation of as-fabricated parts is the anisotropic response that has been documented thoroughly by Kok et al. for additively manufactured materials [41]. Factors such as build orientation and thermal cycling prominently influence the grain structure and mechanical properties, causing heterogeneity in parts produced through powder bed and directed energy deposition processes. However, anisotropy as related to biological response is substantially harder to evaluate and will not be included in this review.

2.3 Types of Porous Implant Structures

A diverse range of lattice geometries can be designed for implant structures. In this work, these are categorized based on their topology/structure into reticulated, stochastic, functionally-graded, or other forms (Figure 1). While the reticulated form is most commonly observed in the literature due to their simple design, there is a growing number of studies that also investigate more complex stochastic lattice geometries. The precise deformation behaviour and mechanical characteristics are dependent on this base structure, where most cellular solids display a simplified three-stage progression of linear elasticity, stress plateauing, and densification [42].

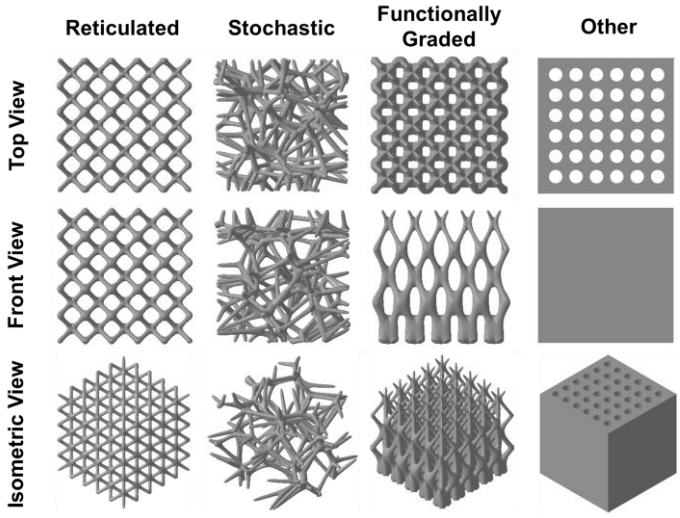

Figure 1: Examples of reticulated, stochastic, functionally-graded, and other porous lattice structures over a short range of unit cells. Reticulated structures have a repeating structure in three directions. Stochastic geometries have no repeating short-order geometry. Functionally-graded and other porous lattices usually have an ordered structure in at least one-direction but have varying properties in one or more directions.

Reticulated lattices describe a unit cell geometry that repeats precisely through the entirety of the structure. Frequently termed ‘regular’ or ‘repeated’ lattices, these structures offer tunable isotropic properties. These are the most common form of lattice in the literature for bone implants and include several geometries such as tetrahedral, octahedral, dodecahedral, or cubic [43]. Since implant stiffness has a geometric dependency, the unit cell strut orientation and porosity have a great impact on mechanical response. Diamond and rhombic dodecahedral lattices, for example,

have been shown to have a lower stiffness than other simple cellular structures but are not able to withstand as much compressive load [44].

Triply-periodic minimal surface (TPMS) unit cells are a subset of reticulated lattices that is becoming increasingly common in the literature. Skeletal or sheet TPMS cells are free from self-intersections and locally minimize surface area by implementing zero mean curvature within the unit cell [45]. Cell migration by durotaxis and the permeable nature of a TPMS geometry suggests that cell migration occurs easier on lattices formed with this zero-mean curvature [46]. In terms of mechanical characterization, TPMS geometries display adequate fatigue properties [47] and have low stiffness while maintaining reasonable peak stress values [48]. Common TPMS geometries include Schwarz diamond, Schwarz primitive, Schwarz gyroid, and Schoen's wrapped package (I-WP) surface (Figure 2). TPMS geometries are in the early stages of exploration for *in vivo* implant applications, where Schwarz primitive structures have been modified to become functionally graded (hybrid) and have been successfully implanted in pigs [49].

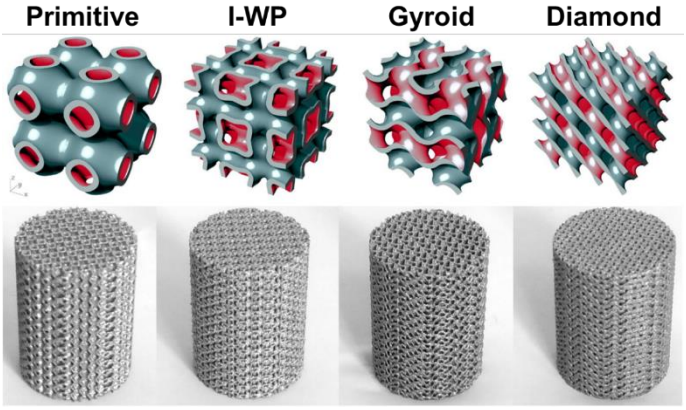

Figure 2: Examples of primitive, I-WP, gyroid, and diamond TPMS lattice structures. These fall under the subset of reticulated lattice. Only recently have TPMS lattices been studied for in vivo bone applications. Adapted from reference [50] *with permission from Elsevier (Copyright 2017).*

Stochastic lattices, also termed 'irregular' or 'trabecular' lattices, have no defined unit cell that repeats through the structure of the lattice. Stochastic lattices typically used biomimicry-derived principles to simulate a trabecular bone structure within the implant geometry. One production method is to analytically-derive struts from a three-dimensional Voronoi tessellation where the porosity and strut thickness can be controlled by the number of seeds and scaling factor [51]. A stochastic lattice geometry can be generated using the Voronoi technique that follows the natural pattern of trabecular bone [52]. Interestingly, the effect of structure on mechanical properties of these trabecular lattices mimics what is seen in trabecular bone [53]. A reduction in strut frequency has a much greater effect on mechanical properties than a comparable porosity increase by reduction of strut thickness [53], where buckling of individual struts in transverse loading becomes more likely as the distance between strut intersections increases. In addition, when designing these lattices, it is important to consider the seed density and three-dimensional isotropy of the base polyhedra to account for bending stresses in vivo. Stochastic lattices may have much more unpredictable short-order response in vivo compared to reticulated lattice structures but the random directional properties for a truly stochastic lattice should average out for larger implants.

Porous foams can also be classified as stochastic lattices due to their lack of regular patterning in the interior of highly porous open-cell specimens. While technically a form of traditional powder metallurgy rather than AM [54], it is also important to briefly consider the response of stochastic foam-like geometries for osseointegration and osteoconduction due to their similarity to other stochastic implants. Due to the rearrangement of the space holder particles during fabrication, these stochastic foams typically have an anisotropic mechanical response [55]. The investigation and processing of porous forms as implant materials is a vast field, and readers interested in this topic are referred elsewhere for more information [56–58].

The problem with classification into reticulated and stochastic structures is the subset of implants that does not fall into either category. Implants with a spatial variation in some property, such as material composition, microstructure, or pore size, constitute an important class known as functionally-graded materials. Functional grading is easily implemented into additive manufacturing processes by modifying the geometry of the CAD model [59], changing processing parameters at different layers during a build, or by changing the composition of the feedstock powder over the course of a build [60]. Since their properties are not the same in the three principal directions but they still have a consistent repeating component, they cannot be classified as either reticulated or stochastic architectures. The weakest point in a functionally-graded material, typically the region with the highest porosity [61], in uniform mechanical loading ultimately dictates the strength of the entire structure. When adapted to complex loads in the body, these emergent types of porous implants may offer the potential to mitigate stress shielding, offer selective bioactivity, and adapt to changes in macroscale bone geometry [62].

Other forms of porous architecture cannot be classified into reticulated or stochastic structures. Micromachined porous channels, for example, lack the 3D repeatability and true randomness of reticulated and stochastic structures, respectively. This type of geometry is often seen in early investigations of porous materials for osteoconduction [63] but are becoming less common as additive manufacturing technologies advance. These other forms of additively manufactured lattice structure (Figure 1, last column) are inclusive to any geometry that cannot be classified as reticulated, stochastic, or functionally-graded.

2.4 Unit Cell Modulation

Many geometric adaptations of porous implants are possible. Two factors that govern the pore distribution through the implant are the strut thickness and the size of the representative unit cell, for which progressive variations are shown in Figure 3 for a reticulated lattice. With a constant unit cell size, increasing the strut size results in a smaller final pore size (all columns, Figure 3). However, increasing the unit cell size while keeping strut size constant results in a larger pore size (all rows, Figure 3). The appearance of pores is also dependent on these factors, where pores can appear more rounded in some instances (e.g. the bottom row, middle column, Figure 3).

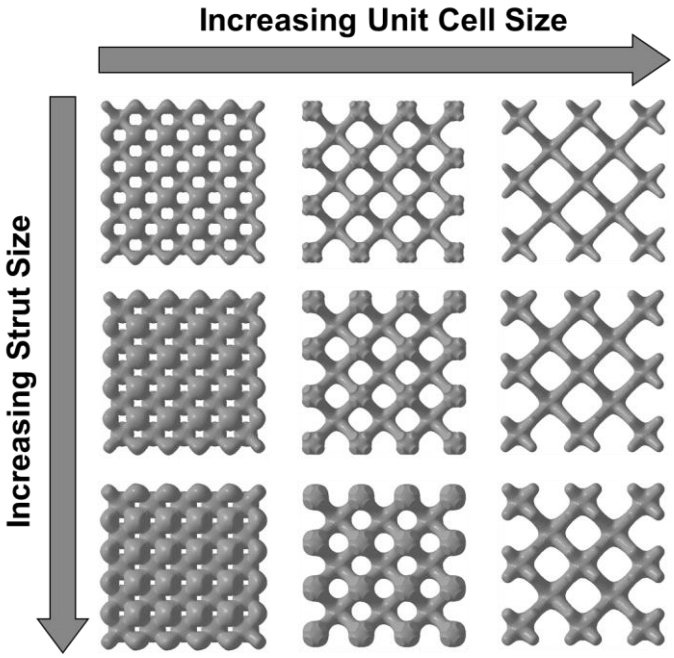

Figure 3: Influence of unit cell size and strut size on pore size and porosity for a reticulated lattice structure. Increasing unit cell size with a constant strut size results in a more porous structure with larger pores. Increasing strut size with a constant unit cell size results in a denser structure with smaller pores.

Models to predict the global mechanical response of some porous implant structures and their associated manufacturing consistency have been systematically investigated [64] to create a design space for tailoring mechanical properties based on the adjustment of strut size and pore size. This information will prove valuable for adjusting design parameters to best match a given anatomical site as more histomorphometric measurements are collected for different pore structures. Where variation in AM processing parameters can also affect the mechanical properties of the implant [65], it may indeed be difficult to isolate mechanical contributions from processing parameters and topological design in process-structure-property relationships. Currently, the precise correlation between strut size, pore size, *in vivo* histology, and *in vivo* histomorphometry has not been defined to definitively declare 'optimum' design parameters for any given clinical or pre-clinical anatomical site. In the papers reviewed in this work this variability is clear, where pore sizes ranged from 50 μm [63] to 1200 μm [66], strut thickness varied from 120 μm [67] to 800 μm [68], and percent porosity ranged from 30% [69] to 83.5% [70].

Geometric factors in a lattice including pore size, net porosity, and strut size can also contribute significantly to the microfluidics for implants in an *in vivo* environment. Bone has a naturally porous network for molecular transport of waste, oxygen, and nutrients [71]. Impairment of this vascular network in bone tissue has been shown to decrease both bone volume fractions and the presence of osteogenic markers [72]. A comparable transport pathway exists as the interconnected pore network of some metallic implants. Work from Warnke et al., for example, has found that *in vitro* culture of osteoblasts can occlude a 450 μm pore after just three weeks of culture. Yet it is important to highlight that *in vitro* culture is not always a predictor of *in vivo* performance [73].The design of the scaffold unit cell in a porous structure is therefore important in ways other than just long-term mechanical consideration. The influence of pore architecture on microfluidics in the

early-stage osteogenesis and angiogenesis of bone tissue should be considered for implant design, especially where predictive tools have been developed in the literature [74]. As will become evident later in this review, certain pore structures can become occluded on their periphery.

3 In *Vivo* Response to AM Metallic Implants

3.1 Commonly Used Animal Models

Due to differences in animal physiology and biomechanics, accurate comparison of *in vivo* osseointegration can be difficult. Threshold strains for periosteal osteogenesis have been shown to differ within a similar anatomical location in a murine model [75], and careful surgical procedures and post-operative management is requisite for intraspecies comparisons of osteogenic data [76]. Critical-sized defects (CSDs) have been standardized as a metric for evaluating *in vivo* osseointegration and are defined as the size of an intraosseous wound that will not spontaneously heal over the lifetime of the animal [77]. CSDs for murine, leporine, canine, caprine, and ovine models have been standardized for some select anatomical locations and observation periods in ASTM F2721, but there is much debate on appropriate sizing for CSDs [78]. For murine femora, the CSD ranges from 5-10 mm with typical endpoints between 8-24 weeks [79]. Ulnar and radial CSDs in leporine bone are defined at 20 mm, with an endpoint of 8-12 weeks [79]. CSDs in canine radii, ulnae, and femora are slightly larger at 21-25 mm with a longer recommended endpoint of 12-24 weeks [79]. CSDs in the tibia of caprine bone should be 26-35 mm, or 25-50 mm in the tibia and metatarsus of ovine bone [79]. For these two models, endpoints should be set at 26 weeks or 16-24 weeks, respectively [79].

Reviews covering the benefits and bone structure of murine, leporine, porcine, and ovine pre-clinical models [80] along with the appropriate defect sizes for several anatomical sites in each model have been done previously [81]. The animal model governs the implant size, which can be especially important in porous AM materials as observation of bone growth into the depth of the implant is reliant on sampling of several sites in the implant. Implants for smaller mammals will naturally contain fewer pores due to the fabrication limits of most AM processes, making systematic sampling more limited. An implant with a pore size of 500 µm and strut size of 250 µm in a critical-sized rat tibial defect, for example, may only have ten pores across its maximum diameter. Where the goal of pre-clinical studies is to predict how implants might behave in humans, measurements of bone homogeneity and penetration depth in a porous implant are limited in their translational capability when considering larger implant sizes in humans.

The selection of pre-clinical animal model is important when considering osseointegration and early osteoconduction since the microscopic bone structure is species-dependent [80] and can therefore differ considerably at different time points. Herein, we will comment on the effect of various lattice structures on the extent of both osseointegration and bone maturity in several pre-clinical models, including the rabbit tibia, rabbit femur, rabbit cranium, goat/sheep metatarsus, pig cranium, and canine dorsal muscle. It is important to note that because of the aforementioned biological differences, a direct comparison of quantitative histomorphometry between species is not possible.

3.2 Observations from Histological Evaluations

At the tissue level, early bone apposition resembles woven bone, where randomly oriented collagen fibrils form during rapid bone modeling [82]. It is also possible to form fibrolamellar bone under rapid growth conditions in fast-growing mammals, birds, or sauropods, where bone is subjected to substantial load [83,84]. This fibrolamellar bone has a unidirectional collagenous orientation but is still mechanically weak relative to more mature, remodelled bone. Finally, after remodelling, lamellar bone has a fixed structure of alternating lamellae, where the orientation of the lamellae alternates between layers [85]. This results in a mechanically mature form of bone *in vivo*. The transition from nascent to mature bone typically has both a strain-dependency [86] and time-dependency as cytokines are expressed differently throughout the remodeling stages [87,88].

Most bone implants are evaluated by histological analyses. Various stains enable an understanding of the biological response to an implant, including the inflammatory response and most importantly the quality of the bone apposition around and within the scaffold. Here, we address some common histological interpretations of bone quality with respect to lattice structures, including fibrous encapsulation, the strain-dependency of osseointegration, bone formation within scaffold pores, and bone maturation.

A common unwanted histological observation following *in vivo* implantation can be the formation of fibrous tissue surrounding or within the scaffold interior. Optimal early-stage *in vivo* conditions for osseointegration includes a fine provisional network of inflammatory tissue for cell signalling [89], mechanical anchorage [89], and neovascularization in the granulation tissue [90] but bulk formation of fibrous tissue through a porous implant can affect physiological loading of bone at the implant surface [91]. Ideally, the fibrous tissue that forms during the initial stage of wound healing as part of the inflammatory response is replaced by bone tissue during osteogenesis [92]. Since osteogenic cells stop migrating after bone matrix secretion has started, the initial fibrin structure is important to allow cells to have a migratory pathway through porous structures [92]. The thickness of the inflammatory fibrous tissue layer is also dictated by the topology of the implant surface [93] in the host response to foreign bodies. Penetration of early fibrovascular tissue into AM titanium lattice interiors has been seen for additively manufactured implants in leporine [94], ovine [39], and caprine [95] bone tissue irrespective of lattice type. In all three of these studies, the net porosity exceeded 60% and fibrovascular tissue was frequently observed at a pore size near 600 µm. This is in agreement with trends in porous bioceramics, where vasculature increases as the minimum pore size increases under similar net porosity (to a maximum investigated diameter of 700 µm) [96].

AM lattice structures, which often have high surface area to volume ratios due to microscale topography, can be especially prone to fibrosis. A study of porous Ti-6Al-4V in porcine crania has shown that the fibrous encapsulation has only allowed for scarce bone-implant contact at the exterior of the implant despite healthy trabecular regeneration in the implant interior, limiting the implant's stability [97]. Unfavourable fibrous encapsulation has been seen to also limit bone-implant contact in a titanium scaffold implanted in an ovine model [39] and murine model [67]. In cases where layers of fibrous tissue prevent bone from anchoring directly to the implant, the long-term integrity of the bone-implant interface is compromised. In terms of other materials, an iron-manganese porous implant exhibited strong bone-implant contact after four weeks in a murine model [98].

Fibrous tissue formation is not always requisite for *de novo* bone formation [37]. In lattice structures, isolated pockets of new bone can form on the scaffold interior in a strain-dependent relationship, where mechanically flexible scaffolds tended to have higher rates of net bone formation on regions within the resected volume [39]. The structure of this bone is also shown to be strain-dependent in the literature, where woven bone readily forms in sham models, but a strain threshold tends to exist for lamellar bone formation in bone defects [86]. Specifically, Claes and Heigele have supposed that there is a certain strain threshold (< 5% strain) for intramembranous ossification to take place during general fracture healing [99]. This strain threshold is an important consideration for lattice optimization, where overly compliant scaffolds may see delayed osteoconduction, but overly stiff scaffolds may see increased stress-shielding.

The typical bone remodeling process forms woven bone during the early stages of osseointegration and gradually replaces it with lamellar bone [100]. However, bone maturation in lattice structures tends to be a more complicated issue. For leporine models, lamellar bone was not observed to form until at least 8 weeks, with woven bone commonly distributed through the lattices as early as 4 weeks [69,94,101,102]. Lattices with higher porosity (herein described as greater than 75%) were also observed to delay bone maturation in leporine models, where the structure of bone through the lattice was predominantly woven bone after 8 weeks and lamellar bone was not visible until at least 16 weeks [103]. Overall, formation of lamellar bone in larger mammals will tend to be slower than in smaller mammals within the scaffold interior as the remodelling process as a whole is shorter in small mammals [104]. While insufficient data exists to validate the relationship between maturation rate and porosity in canine, ovine, and caprine models, there are benchmarks set for each in the present literature. In canine models, woven bone dominates the structure of highly porous metallic implants after 8 weeks and shows signs of maturation at 16 weeks [105]. For low-porosity implants in caprine models, limited woven bone is present after 12 weeks with a greater amount of woven bone present after 26 weeks [95]. The woven to lamellar transition in this study was between the 26-week and 52-week timepoints in this caprine study [95]. Titanium scaffolds in an ovine model displayed predominantly woven bone after 6 weeks, but similar polyamide control scaffolds showed regions of woven bone sandwiched between lamellar bone [39]. At the cellular level, Shah et al. have noted a net increase in ovine osteocyte density at the interface of EBM porous constructs compared to fully dense specimens [68]. This may be attributed to a high rate of initial osteoblast adhesion to the implant surface, or to high turnover rates to create an apparent ‘less-aged’ bone structure at the interface of the porous structure [68]. Raman spectroscopy had indicated in this study that there was increased maturity at the interface of the porous structure by comparing the CO_3^{2-}/PO_4^{3-} peak ratio [68].

In general, however, it is important to note that bone maturation depends strongly on the implant location and animal model, rather than the AM scaffold design or implant chemistry. Despite limitations in implant comparison from study to study, the interplay of design criteria such as pore size and porosity were shown to influence intraspecies bone maturation and quantity of fibrovascular tissue at early stages of implantation. Implants with a target pore geometry of roughly 600 µm and porosity of 75% should provide an adequate balance between these two simultaneous processes during bone regeneration, although much of this conclusion stems from leporine histology data.

3.3 Defining Common Histomorphometric Parameters

The most common quantitative factors extracted from histomorphometry to characterize osseointegration are bone volume per total volume, bone area and bone-implant contact. Bone volume density (BV/TV) is a common way of quantifying osseointegration by measuring the ratio of bone tissue volume to total volume using micro-computed tomography [106]. Bone area (BA) is an equivalent 2D measurement that measures the area of new bone growth over the total area available for bone ingrowth within a region of interest surrounding or inside a scaffold [106]. Similarly, bone-implant contact (BIC) measures the length of direct bone contact along an implant, usually presented as a percentage of the total length available. Implant stability in pre-clinical models can be evaluated by measuring the BIC, and correlating this to mechanical testing methods, including pull-out force, push-out force, or removal torque. Pull-out and push-out tests measure the required force to remove an implanted structure, although the results between the two are not always directly comparable [107]. Lastly, removal torque tests are an alternative way to measure bone-implant anchorage by evaluating the required torque to remove a threaded screw from its implant site. While other histomorphometric parameters exist for specific applications, the ones listed above are most abundant in the literature.

However, in AM, due to the lack of bone ubiquity through most lattice structures, it has become increasingly common practice to segment the implant into distinct regions for histomorphometry, since bone volume tends to be higher at the scaffold exterior. Therefore, histomorphometric measurements at the early stage of bone ingrowth in AM lattices are regularly supplemented by segmenting into distinct inner/outer lattice regions, but consistency in this volumetric segmentation is lacking across the literature. For example, Palmquist et al. separate 2D sub-regions into three vertical ‘zones’ and three horizontal ‘levels’ for calculation of BV/TV and BIC [108]. Alternatively, Reznikov et al. assigned a scoring system to define bone-implant contact for evenly-spaced micro-computed tomography slices from the periosteal surface inwards, with a manually-defined boundary between the scaffold interior and exterior [39]. Where most *in vivo* trials have been performed in small mammals, such as rats and rabbits, the problem of bone nucleation on a scaffold interior may amplify when scaling up for clinical application in larger mammals, and this would represent a decrease in measured BIC or BA, which are often related to osteoconduction. For example. existing pre-clinical models in larger mammals, such as ovine, have shown slower osteoconduction through the porous structures, where bone area on the interior third of the scaffold is approximately half of the outer third [108]. In addition, where porous networks for larger implants may have the same lattice structures as their smaller counterparts, the bulk BV/TV ratio may decrease if the bone penetration depth stagnates or slows for a specific geometry, defect size, or animal model.

Understanding the interplay between unit cell structure, implant stiffness, and resulting osseointegration is important for *in vivo* success. Where a wealth of *in vitro* and compression data exists for various lattice designs [48,109–111], there is little information describing these relationships quantitatively and systematically during *in vivo* studies. Due to variability in experimental techniques (e.g. animal type, anatomical location, implantation time, implant size, pore morphology, pore size, etc.), only qualitative observations can be critically analyzed from study to study. For this reason, we have little information about the ‘ideal’ lattice structure for osseointegration and osteoconduction. Table 1 and Table 2 attempt to sort the histomorphometric

and mechanical findings in the literature by the predominant geometrical parameters: pore size and percent porosity, respectively.

Table 1: Trends in osseointegration with pore size for various pre-clinical animal models. Bone-implant contact (BIC), bone area (BA), bone volume fraction (BV/TV), pull-out force, or push-out force serve as the most common techniques for quantifying osseointegration of lattice geometries. In all cases, increasing implantation time shows an increased value in at least one of these metrics.

Pore Size (μm)	Pre-Clinical Model	Implantation Time/Type	BIC (%)	BA (%)	BV/TV (%)	Pull-Out Force (N)	Push-Out Force (N) or Push-Out Stress (MPa)	Reference
100-200	Leporine	8 wk^{CPT-S}	-	26, 30	-	-	-	[69]
200-300	Leporine	2 wk^{CPT-R}	-	-	-	38	-	[94]
		4 wk^{CPT-R}	-	-	-	126	-	[94]
		8 wk$^{CPT-R/S}$	47	29, 36	-	115	-	[69,94,112]
300-400	Leporine	4 wk^{CPT-R}	-	30	-	-	-	[113]
		8 wk^{CPT-R}	35	32	-	-	-	[112]
	Caprine	12.5 wk^{Ti64-R}	-	1	-	-	-	[95]
		25.5 wk^{Ti64-R}	-	17	-	-	-	[95]
		51 wk^{Ti64-R}	-	25	-	-	-	[95]
400-500	Leporine	2 wk$^{R/S}$	-	12, 27, 23, 24	-	-	140, 221, 181, 219	[114]
		4 wk$^{CPT/Ti64-R/S}$	-	20, 30, 32, 34, 34	-	-	2.8 [MPa], 362, 372, 419, 434	[113–115]
		7 wk$^{R/S}$	-	24, 33, 36, 37	-	-	401, 419, 473, 492	[114]
		12 wk^{Ti64-R}	-	-	-	-	3.6 [MPa]	[115]
	Porcine	2 wk^{Ti64-R}	0.5	-	5.6	-	-	[97]
		4 wk^{Ti64-R}	4.1	-	13.8	-	-	[97]
		8.5 wk^{Ti64-R}	6.0	-	34.2	-	-	[97]
500-600	Leporine	2 wk^{CPT-R}	-	-	-	68	-	[94]
		4 wk^{CPT-R}	-	-	-	147	-	[94]
		8 wk^{CPT-R}	39	31	19	157	-	[70,94,112]
	Canine	16 wk^{CPT-O}	-	8	-	-	-	[66]
		26 wk^{CPT-O}	-	18	-	-	-	[66]
		52 wk^{CPT-O}	-	25	-	-	-	[66]

$^{-}$ Data not available; ^{CPT} Commercially-pure titanium; ^{Ti64} Ti-6Al-4V; ^{R} Reticulated; ^{S} Stochastic; ^{O} Other

Pore Size (μm)	Pre-Clinical Model	Implantation Time/Type	BIC (%)	BA (%)	BV/TV (%)	Pull-Out Force (N)	Push-Out Force (N) or Push-Out Stress (MPa)	Reference
600-700	Leporine	4 wk$^{Ti64\text{-}R}$	-	-	-	-	3.2 [MPa]	[115]
		8 wk$^{CPT\text{-}R}$	37, 50	28, 30	15, 25	-	-	[70,112]
		12 wk$^{Ti64\text{-}R}$	-	-	-	-	4.3 [MPa]	[115]
	Canine	16 wk$^{CPT\text{-}O}$	-	8	-	-	-	[66]
		26 wk$^{CPT\text{-}O}$	-	14	-	-	-	[66]
		52 wk$^{CPT\text{-}O}$	-	19	-	-	-	[66]
800-900	Leporine	2 wk$^{CPT\text{-}R}$	-	-	-	33	-	[94]
		3 wk$^{CPT\text{-}R}$	23	-	18	-	-	[116]
		4 wk$^{CPT/Ti64\text{-}R}$	-	52	-	127	2.9 [MPa]	[94,113,115]
		8 wk$^{CPT\text{-}R}$	31	-	14	131	-	[94,116]
		12 wk$^{Ti64\text{-}R}$	-	-	-	-	3.9 [MPa]	[115]
900-1000	Canine	16 wk$^{CPT\text{-}O}$	-	3	-	-	-	[66]
		26 wk$^{CPT\text{-}O}$	-	5	-	-	-	[66]
		52 wk$^{CPT\text{-}O}$	-	12	-	-	-	[66]
> 1000	Leporine	3 wk$^{CPT\text{-}R}$	38	-	24	-	-	[116]
		4 wk$^{CPT\text{-}R}$	-	39	-	-	-	[113]
		8 wk$^{CPT\text{-}R}$	30	-	10	-	-	[116]
	Canine	16 wk$^{CPT\text{-}O}$	-	2	-	-	-	[66]
		26 wk$^{CPT\text{-}O}$	-	4	-	-	-	[66]
		52 wk$^{CPT\text{-}O}$	-	7	-	-	-	[66]

$^{-}$ Data not available; ^{CPT} Commercially-pure titanium; ^{Ti64} Ti-6Al-4V; ^{R} Reticulated; ^{S} Stochastic; ^{O} Other

3.4 Observations from Histomorphometric Evaluations

In general, porous AM implants have been observed to outperform solid controls in various forms of bone histomorphometry [101,112,114,117], but which lattice geometries perform the best is still unknown. Wang et al. have proven that unit cell structure for reticulated lattices can influence bone growth kinetics, where diamond-based lattice structures caused higher bone area fractions than tetrahedral lattice structures [114].Wieding et al. have similarly modified a porous structure to find that a simple reticulated cubic lattice showed less bone ingrowth than a hollow cage structure with angled struts [118]. In contrast, de Wild et al. have observed that osseointegration and osteoconduction occur independent of unit cell architecture [112]. By changing the strut thickness or unit cell dimensions of any lattice structure, there is a change in local stiffness through the implant. Since nascent bone tends to be locally strained depending on implant stiffness, further *in vivo* investigation into lattice geometry is necessary to evaluate the optimal lattice structure and perhaps appropriate functional grading for bone implants. As a reference, the implanted scaffolds summarized in this work have an apparent modulus that varies from 0.6-38 GPa, with the vast majority having a modulus under 10 GPa.

The pore size in a lattice structure appears to be a dominant factor affecting osseointegration and *in vivo* mechanical stability. Table 1 summarizes quantitative findings for bone ingrowth and stability for porous implants depending on pore size for several pre-clinical models. Optimal pore size for orthopaedic applications was first documented to range from 50-400 μm for maximum fixation strength [119]. While a pore size in this range may be correlated to good mechanical anchorage, it is important to note that there may be no minimum pore size for the onset of osseointegration within the current manufacturing limitations of additive manufacturing. Itälä et al., for example, monitored osseointegration into 50 μm machined cylindrical holes and found secondary osteonal structures present in a leporine model [102]. Defining an upper bound for pore size is more difficult. Fukuda et al. has noted that square pores with a diagonal length of 500 μm outperformed larger pores (600 μm, 900 μm, and 1200 μm) in terms of bone penetration depth and BA for a canine model [66]. In contrast to this, cylindrical pores with a diameter of 900 μm in an AM structure displayed greater bone volumes than pores with diameters of 500 μm and 700 μm in a canine model [115]. This canine study, however, had also shown that trabeculae thickness in the new bone was highest for the 500 μm grouping [115], reiterating that sometimes not only bone quantity but quality are important predictors of implant success. In a study that examined porous metallic structures with smaller pores, it was found that increasing pore size resulted in a higher interfacial bone fraction up to the largest pores (300 μm) [69]. A recent work has attempted to investigate the effect of systematically modifying both strut size and strut spacing in rabbit crania [113]. This study finds statistically higher BA percentages for a strut spacing of 800 μm compared to alternate spacings of 500 μm and 1800 μm after four weeks of implantation, but indeterminate results in terms of bone bridging and histomorphometry associated with strut diameter. As a whole, trends in the literature reveal that osseointegration and osteoconduction are most favourable in the pore size range of 300-500 μm, but contrasting studies implicate this could be marginally higher based on unknown confounding factors or experimental design of pre-clinical trials. The translation from pre-clinical to clinical model should also consider the rate of bone apposition in humans relative to any given pre-clinical model if pore occlusion effects are to be considered significant.

The other factor greatly affecting osseointegration is the percent (%) porosity. Table 2 expresses bone formation and implant stability with respect to porosity. There is a distinct lack of information about correlating implant stability in highly porous (> 75% porosity) metallic implants to net porosity in a quantitative regard, as few systematic trials have been conducted to evaluate the percent porosity by keeping a constant pore size. Li et al., for example, evaluated *in vitro* response with respect to pore size (300-400 µm, 400-500 µm, 500-700 µm) in their specimens by keeping the same porosity [95], but did not do correlative *in vivo* experiments on two of the study groups. Meanwhile, de Wild's work on highly porous scaffolds (70-90% porosity) show remarkably high values of bone-implant contact compared to other porosity values and therefore excellent potential for osteoconduction [112]. The interplay between unit cell size, pore size, and porosity in the geometric design of scaffolds makes it difficult to isolate the *in vivo* response to a particular geometric variable, but instead highlights the importance of considering all three simultaneously for lattice design. In terms of novel materials, tantalum scaffolds have shown better bone-implant contact than titanium, with a higher fraction of early osteoid and a lack of early interfacial gaps in the bone-implant interface [120]. In general, implants of any type with a percent porosity in the range of 50-70% showed reasonable osseointegration, where lower measurements of BIC, BA, or BV/TV were observed outside of this range.

Table 2: Select histomorphometric observations with respect to % porosity and pre-clinical model for implanted AM lattices. Bone-implant contact (BIC), bone area (BA), bone volume fraction (BV/TV), pull-out force, or push-out force serve as the most common techniques for quantifying osseointegration of lattice geometries.

Porosity (%)	Pre-Clinical Model	Implantation Time/Type	BIC (%)	BA (%)	BV/TV (%)	Pull-Out Force (N)	Push-Out Force (N) or Push-Out Stress (MPa)	Reference
30-40	Leporine	8 wk^{CPT-S}	-	26, 29	-	-	-	[69]
	Caprine	12.5 wk^{Ti64-R}	-	1	-	-	-	[95]
		25.5 wk^{Ti64-R}	-	7	-	-	-	[95]
		51 wk^{Ti64-R}	-	25	-	-	-	[95]
40-50	Leporine	4 wk^{Ti64-R}	-	-	-	-	2.8 [MPa]	[115]
		8 wk^{CPT-S}	-	30	-	-	-	[69]
		12 wk^{Ti64-R}	-	-	-	-	3.6 [MPa]	[115]
50-60	Leporine	3 wk^{CPT-R}	38	-	24	-	-	[116]
		4 wk^{Ti64-R}	-	-	-	-	2.9 [MPa]	[115]
		8 wk^{CPT-R}	30	-	10	-	-	[116]
		12 wk^{Ti64-R}	-	-	-	-	3.9 [MPa], 4.3 [MPa]	[115]
	Ovine	12 wk^{O}	-	-	20, 43	-	-	[117]
60-70	Leporine	2 wk$^{CPT-R/S}$	-	12, 23, 24, 27	-	33, 38, 68	140, 181, 219, 221	[114]
		3 wk^{CPT-R}	23	-	18	-	-	[116]
		4 wk$^{CPT-R/S}$	-	20, 30, 34, 34	-	126, 127, 147	362, 372, 419, 434	[94,114]
		7 wk$^{R/S}$	-	24, 33, 37	-	-	401, 419, 473	[114]
		8 wk^{CPT-R}	31	-	14	115, 131, 157	-	[94,116]
	Porcine	2 wk^{Ti64-R}	0.47	-	5.6	-	-	[97]
		4 wk^{Ti64-R}	4.14	-	13.8	-	-	[97]
		8.5 wk^{Ti64-R}	5.96	-	34.2	-	-	[97]
	Ovine	6 wk^{CPT-R}	-	-	6.9	-	-	[39]
70-80	Leporine	8 wk^{CPT-R}	35, 37, 47	30, 32, 36	-	-	-	[112]
80-90	Leporine	8 wk^{CPT-R}	39, 50	28, 31	15, 19, 25	-	-	[70,112]
	Ovine	6 wk^{CPT-S}	-	-	9.4	-	-	[39]

$^{-}$ Data not available; ^{CPT} Commercially-pure titanium; ^{Ti64} Ti-6Al-4V; ^{R} Reticulated; ^{S} Stochastic; ^{O} Other

4 Conclusions

As additive manufacturing has become more commonplace in the field of metallic implant production, it is increasingly important to evaluate the performance of complex geometries in pre-clinical *in vivo* models. This review surveyed existing studies to make general conclusions about the *in vivo* performance of AM metallic lattice structures based on histological and histomorphometric data. For lattice structures, geometric considerations such as strut thickness and unit cell size dictate the resulting pore size and percent porosity of the implant. This review notes a clear lack in the present literature on systematic evaluation of AM implant designs to identify an optimum pore architecture and size for osseointegration in critical-sized bone defects. However, we find that the most common form of porous AM implant studied *in vivo* tends to have a reticulated lattice structure, with a pore size ranging from 400-500 μm and percent porosity ranging between 60-70%. Most of these implants have been made of titanium alloys and are produced by selective laser melting. There have been few studies to systematically evaluate the effects of other pore structures, such as stochastic/trabecular architectures, and therefore, we cannot speculate if any given reticulated structure with this pore structure is best, or simply the most widely investigated. From the studies evaluated in this review, porosity seems to correlate strongly to bone maturity (where porosity between 50-70% trended towards larger amounts of lamellar bone in the pore network), while pore size may be more closely related to the mechanical stability of the implant (where increased values of BIC, pull-out force, and push-out force were correlated to pore sizes between 300-500 μm). Early onset of woven-to-lamellar transition and formation of favourable precursory fibrovascular tissue is most common in implants with a pore size of around 600 μm and a porosity of 75%.

Lastly, where many publications modify lattice geometry from a mechanical perspective to lower implant stiffness, it is our opinion that future work should perhaps shift to developing strategies for improved integration of high-quality bone tissue throughout the interior of the implant. For example, in almost all cases reported in this review, complete penetration of bone throughout the lattice interior was lacking. While this review did not broach the topic of surface modification for AM due to a lack of publications reporting *in vivo* performance, considerable literature citing *in vitro* methods for modifying implant pore chemistry and topography is available, including acid etching [70], sandblasting [70], micro-arc oxidation [121], dip coating [122], or other methods [123]. Surface modification approaches to regulate osteoconduction, which are widely effective on conventionally cast porous and non-porous metallic implants [124–126], should receive more attention, especially in a systematic manner to compare their efficacy when applied to the interior of a porous implant.

5 Acknowledgements

This work was supported by the Natural Sciences and Engineering Research Council of Canada (RGPIN-2014-06-053) and by the Foshan Science and Technology Innovation Project (No. 2018IT100212). JD is supported by a NSERC PGS-D scholarship.

6 Author Contributions

J. Deering: Conceptualization, Data Curation, Formal Analysis, Writing – Original Draft, Writing – Review & Editing

K. Grandfield: Conceptualization, Funding Acquisition, Supervision, Writing – Review & Editing

7 Conflicts of Interest

The authors declare no conflict of interest.

8 References

1. Albrektsson T, Johansson C. Osteoinduction, osteoconduction and osseointegration. Eur Spine J. 2001;10(Suppl 2):S96–101.

2. Huiskes R, Weinans H, van Rietbergen B. The Relationship Between Stress Shielding and Bone Resorption Around Total Hip Stems and the Effects of Flexible Materials. Clin Orthop Relat R. 1992;274(NA;):124–34.

3. Ashby MF, Medalist RFM. The mechanical properties of cellular solids. Metallurgical Transactions. 1983;14(9):1755–69.

4. Choren JA, Heinrich SM, Silver-Thorn MB. Young's modulus and volume porosity relationships for additive manufacturing applications. J Mater Sci. 2013;48(15):5103–12.

5. Hao Y-L, Li S-J, Yang R. Biomedical titanium alloys and their additive manufacturing. Rare Metals. 2016;35(9):661–71.

6. Karre R, Niranjan MK, Dey SR. First principles theoretical investigations of low Young's modulus beta Ti–Nb and Ti–Nb–Zr alloys compositions for biomedical applications. Mater Sci Eng C. 2015;50:52–8.

7. Luo JP, Sun JF, Huang YJ, Zhang JH, Zhang YD, Zhao DP, Yan M. Low-modulus biomedical Ti–30Nb–5Ta–3Zr additively manufactured by Selective Laser Melting and its biocompatibility. Mater Sci Eng C. 2018;97(Mater. Sci. Eng. R 47 3 2004):275–84.

8. Yilmazer H, Niinomi M, Nakai M, Cho K, Hieda J, Todaka Y, Miyazaki T. Mechanical properties of a medical β-type titanium alloy with specific microstructural evolution through high-pressure torsion. Mater Sci Eng C. 2013;33(5):2499–507.

9. Niinomi M, Nakai M, Hieda J. Development of new metallic alloys for biomedical applications. Acta Biomater. 2012;8(11):3888–903.

10. Schulze C, Weinmann M, Schweigel C, Keßler O, Bader R. Mechanical Properties of a Newly Additive Manufactured Implant Material Based on Ti-42Nb. Materials. 2018;11(1):124.

11. Krishna BV, Bose S, Bandyopadhyay A. Low stiffness porous Ti structures for load-bearing implants. Acta Biomater. 2007;3(6):997–1006.

12. Xin XZ, Xiang N, Chen J, Wei B. In vitro biocompatibility of Co–Cr alloy fabricated by selective laser melting or traditional casting techniques. Mater Lett. 2012;88:101–3.

13. Hazlehurst K, Wang CJ, Stanford M. Evaluation of the stiffness characteristics of square pore CoCrMo cellular structures manufactured using laser melting technology for potential orthopaedic applications. Mater Design. 2013;51:949–55.

14. Sing SL, An J, Yeong WY, Wiria FE. Laser and electron-beam powder-bed additive manufacturing of metallic implants: A review on processes, materials and designs. J Orthopaed Res. 2015;34(3):369–85.

15. Li Y, Jahr H, Zhou J, Zadpoor AA. Additively manufactured biodegradable porous metals. Acta Biomater. 2020;115:29–50.

16. Wang Z, Wang C, Li C, Qin Y, Zhong L, Chen B, Li Z, Liu H, Chang F, Wang J. Analysis of factors influencing bone ingrowth into three-dimensional printed porous metal scaffolds: A review. J Alloy Compd. 2017;717:271–85.

17. Wang X, Xu S, Zhou S, Xu W, Leary M, Choong P, Qian M, Brandt M, Xie YM. Topological design and additive manufacturing of porous metals for bone scaffolds and orthopaedic implants: A review. Biomaterials. 2016;83:127–41.

18. Zok FW. Integrating lattice materials science into the traditional processing–structure–properties paradigm. Mrs Commun. 2019;9(4):1284–91.

19. Weber FE. Reconsidering Osteoconduction in the Era of Additive Manufacturing. Tissue Eng Part B Rev. 2019;25(5):375–86.

20. Frazier WE. Metal Additive Manufacturing: A Review. J Mater Eng Perform. 2014;23(6):1917–28.

21. Wong KV, Hernandez A. A Review of Additive Manufacturing. Isrn Mech Eng. 2012;2012:1–10.

22. Bikas H, Stavropoulos P, Chryssolouris G. Additive manufacturing methods and modelling approaches: a critical review. Int J Adv Manuf Technology. 2016;83(1–4):389–405.

23. Mullen L, Stamp RC, Brooks WK, Jones E, Sutcliffe CJ. Selective Laser Melting: A regular unit cell approach for the manufacture of porous, titanium, bone in-growth constructs, suitable for orthopedic applications. J Biomed Mater Res Part B Appl Biomaterials. 2009;89B(2):325–34.

24. Guo Q, Zhao C, Qu M, Xiong L, Escano LI, Hojjatzadeh SMH, Parab ND, Fezzaa K, Everhart W, Sun T, Chen L. In-situ characterization and quantification of melt pool variation under constant input energy density in laser powder-bed fusion additive manufacturing process. Addit Manuf. 2019;28:600–9.

25. Qiu C, Yue S, Adkins NJE, Ward M, Hassanin H, Lee PD, Withers PJ, Attallah MM. Influence of processing conditions on strut structure and compressive properties of cellular lattice structures fabricated by selective laser melting. Mater Sci Eng. 2015;628(Prog. Mater. Sci. 46 2001):188–97.

26. Liu Y, Yang Y, Mai S, Wang D, Song C. Investigation into spatter behavior during selective laser melting of AISI 316L stainless steel powder. Mater Design. 2015;87:797–806.

27. Ghouse S, Babu S, Arkel RJV, Nai K, Hooper PA, Jeffers JRT. The influence of laser parameters and scanning strategies on the mechanical properties of a stochastic porous material. Mater Design. 2017;131(J. Biomed. Mater. Res. B Appl. Biomater. 89B 2 2009):498–508.

28. Weißmann V, Drescher P, Bader R, Seitz H, Hansmann H, Laufer N. Comparison of Single Ti6Al4V Struts Made Using Selective Laser Melting and Electron Beam Melting Subject to Part Orientation. Metals-basel. 2017;7(3):91.

29. Wang L, Felicelli SD, Pratt P. Residual stresses in LENS-deposited AISI 410 stainless steel plates. Mater Sci Eng. 2008;496(1–2):234–41.

30. Rangaswamy P, Holden TM, Rogge RB, Griffith ML. Residual stresses in components formed by the laserengineered net shaping (LENS®) process. J Strain Analysis Eng Des. 2003;38(6):519–27.

31. Yuan L, Ding S, Wen C. Additive manufacturing technology for porous metal implant applications and triple minimal surface structures: A review. Bioact Mater. 2019;4(1):56–70.

32. Kreitcberg A, Brailovski V, Prokoshkin S. New biocompatible near-beta Ti-Zr-Nb alloy processed by laser powder bed fusion: Process optimization. J Mater Process Tech. 2018;252:821–9.

33. Mehjabeen A, Song T, Xu W, Tang HP, Qian M. Zirconium Alloys for Orthopaedic and Dental Applications. Adv Eng Mater. 2018;20(9):1800207.

34. Niinomi M, Liu Y, Nakai M, Liu H, Li H. Biomedical titanium alloys with Young's moduli close to that of cortical bone. Regen Biomaterials. 2016;3(3):173–85.

35. Ozan S, Lin J, Li Y, Wen C. New Ti-Ta-Zr-Nb alloys with ultrahigh strength for potential orthopedic implant applications. J Mech Behav Biomed. 2017;75:119–27.

36. Long M, Rack HJ. Titanium alloys in total joint replacement—a materials science perspective. Biomaterials. 1998;19(18):1621–39.

37. Kujala S, Ryhänen J, Danilov A, Tuukkanen J. Effect of porosity on the osteointegration and bone ingrowth of a weight-bearing nickel–titanium bone graft substitute. Biomaterials. 2003;24(25):4691–7.

38. Ayers RA, Simske SJ, Bateman TA, Petkus A, Sachdeva RLC, Gyunter VE. Effect of nitinol implant porosity on cranial bone ingrowth and apposition after 6 weeks. J Biomed Mater Res. 1999;45(1):42–7.

39. Reznikov N, Boughton OR, Ghouse S, Weston AE, Collinson L, Blunn GW, Jeffers J, Cobb JP, Stevens MM. Individual response variations in scaffold-guided bone regeneration are determined by independent strain- and injury-induced mechanisms. Biomaterials. 2018;194(J. Bone Joint Surg. Am. 89 Suppl 3 2007):183–94.

40. Alvarez K, Hyun S-K, Nakano T, Umakoshi Y, Nakajima H. In vivo osteocompatibility of lotus-type porous nickel-free stainless steel in rats. Mater Sci Eng C. 2009;29(4):1182–90.

41. Kok Y, Tan XP, Wang P, Nai MLS, Loh NH, Liu E, Tor SB. Anisotropy and heterogeneity of microstructure and mechanical properties in metal additive manufacturing: A critical review. Mater Design. 2018;139:565–86.

42. Gibson LJ. Biomechanics of cellular solids. J Biomech. 2005;38(3):377–99.

43. Mahmoud D, Elbestawi MA. Lattice Structures and Functionally Graded Materials Applications in Additive Manufacturing of Orthopedic Implants: A Review. J Manuf Mater Process. 2017;1(2):13.

44. Ahmadi SM, Yavari SA, Wauthle R, Pouran B, Schrooten J, Weinans H, Zadpoor AA. Additively Manufactured Open-Cell Porous Biomaterials Made from Six Different Space-Filling Unit Cells: The Mechanical and Morphological Properties. Materials. 2015;8(4):1871–96.

45. Kapfer SC, Hyde ST, Mecke K, Arns CH, Schröder-Turk GE. Minimal surface scaffold designs for tissue engineering. Biomaterials. 2011;32(29):6875–82.

46. Rajagopalan S, Robb RA. Schwarz meets Schwann: Design and fabrication of biomorphic and durataxic tissue engineering scaffolds. Med Image Anal. 2006;10(5):693–712.

47. Kelly CN, Francovich J, Julmi S, Safranski D, Guldberg RE, Maier HJ, Gall K. Fatigue Behavior of As-Built Selective Laser Melted Titanium Scaffolds with Sheet-based Gyroid Microarchitecture for Bone Tissue Engineering. Acta Biomater. 2019;94:610–26.

48. Al-Ketan O, Rowshan R, Al-Rub RKA. Topology-mechanical property relationship of 3D printed strut, skeletal, and sheet based periodic metallic cellular materials. Addit Manuf. 2018;19(Acta Biomater. 4 2008):167–83.

49. Li L, Shi J, Zhang K, Yang L, Yu F, Zhu L, Liang H, Wang X, Jiang Q. Early osteointegration evaluation of porous Ti6Al4V scaffolds designed based on triply periodic minimal surface models. J Orthop Transl. 2019;(BMC Muscoskelet Disord 18 2017).

50. Bobbert FSL, Lietaert K, Eftekhari AA, Pouran B, Ahmadi SM, Weinans H, Zadpoor AA. Additively manufactured metallic porous biomaterials based on minimal surfaces: A unique combination of topological, mechanical, and mass transport properties. Acta Biomater. 2017;53(J. Biomech. 45 6 2012):572–84.

51. Fantini M, Curto M, Crescenzio FD. A method to design biomimetic scaffolds for bone tissue engineering based on Voronoi lattices. Virtual Phys Prototyp. 2016;11(2):77–90.

52. Liang H, Yang Y, Xie D, Li L, Mao N, Wang C, Tian Z, Jiang Q, Shen L. Trabecular-like Ti-6Al-4V scaffolds for orthopedic: fabrication by selective laser melting and in vitro biocompatibility. J Mater Sci Technol. 2019;35(Der Unfallchirurg 109 2006):1284–97.

53. Silva MJ, Gibson LJ. Modeling the mechanical behavior of vertebral trabecular bone: Effects of age-related changes in microstructure. Bone. 1997;21(2):191–9.

54. Ryan G, Pandit A, Apatsidis DP. Fabrication methods of porous metals for use in orthopaedic applications. Biomaterials. 2006;27(13):2651–70.

55. Imwinkelried T. Mechanical properties of open-pore titanium foam. J Biomed Mater Res A. 2007;81A(4):964–70.

56. Yu C-J, Eifert HH, Banhart J, Baumeister J. Metal foaming by a powder metallurgy method: Production, properties and applications. Material Res Innovations. 1998;2(3):181–8.

57. Singh S, Bhatnagar N. A survey of fabrication and application of metallic foams (1925–2017). J Porous Mat. 2018;25(2):537–54.

58. Wen CE, Yamada Y, Shimojima K, Chino Y, Asahina T, Mabuchi M. Processing and mechanical properties of autogenous titanium implant materials. J Mater Sci Mater Medicine. 2002;13(4):397–401.

59. Mahmoud D, Elbestawi MA, Yu B. Process–Structure–Property Relationships in Selective Laser Melting of Porosity Graded Gyroids. J Medical Devices. 2019;13(3):031005.

60. Shishkovsky I, Missemer F, Smurov I. Direct Metal Deposition of Functional Graded Structures in Ti- Al System. Physcs Proc. 2012;39:382–91.

61. Fousová M, Vojtěch D, Kubásek J, Jablonská E, Fojt J. Promising characteristics of gradient porosity Ti-6Al-4V alloy prepared by SLM process. J Mech Behav Biomed. 2017;69:368–76.

62. Sola A, Bellucci D, Cannillo V. Functionally graded materials for orthopedic applications – an update on design and manufacturing. Biotechnol Adv. 2016;34(5):504–31.

63. Itälä AI, Ylänen HO, Ekholm C, Karlsson KH, Aro HT. Pore diameter of more than 100 μm is not requisite for bone ingrowth in rabbits. J Biomed Mater Res. 2001;58(6):679–83.

64. Melancon D, Bagheri ZS, Johnston RB, Liu L, Tanzer M, Pasini D. Mechanical characterization of structurally porous biomaterials built via additive manufacturing: experiments, predictive models, and design maps for load-bearing bone replacement implants. Acta Biomater. 2017;63:350–68.

65. Tsopanos S, Mines RAW, McKown S, Shen Y, Cantwell WJ, Brooks W, Sutcliffe CJ. The Influence of Processing Parameters on the Mechanical Properties of Selectively Laser Melted Stainless Steel Microlattice Structures. J Manuf Sci Eng. 2010;132(4):041011.

66. Fukuda A, Takemoto M, Saito T, Fujibayashi S, Neo M, Pattanayak DK, Matsushita T, Sasaki K, Nishida N, Kokubo T, Nakamura T. Osteoinduction of porous Ti implants with a channel structure fabricated by selective laser melting. Acta Biomater. 2011;7(5):2327–36.

67. Stok JV der, Jagt OPV der, Yavari SA, Haas MFPD, Waarsing JH, Jahr H, Lieshout EMMV, Patka P, Verhaar JAN, Zadpoor AA, Weinans H. Selective laser melting-produced porous titanium scaffolds regenerate bone in critical size cortical bone defects. J Orthopaed Res. 2013;31(5):792–9.

68. Shah FA, Snis A, Matic A, Thomsen P, Palmquist A. 3D printed Ti6Al4V implant surface promotes bone maturation and retains a higher density of less aged osteocytes at the bone-implant interface. Acta Biomater. 2016;30(Biomaterials 27 2006):357–67.

69. de Vasconcellos LMR, Leite DO, Oliveira FN de, Carvalho YR, Cairo CAA. Evaluation of bone ingrowth into porous titanium implant: histomorphometric analysis in rabbits. Braz Oral Res. 2010;24(4):399–405.

70. de Wild M, Schumacher R, Mayer K, Schkommodau E, Thoma D, Bredell M, Gujer AK, Grätz KW, Weber FE. Bone Regeneration by the Osteoconductivity of Porous Titanium Implants Manufactured by Selective Laser Melting: A Histological and Micro Computed Tomography Study in the Rabbit. Tissue Eng Pt A. 2013;19(23–24):2645–54.

71. Hollister SJ. Porous scaffold design for tissue engineering. Nat Mater. 2005;4(7):518–24.

72. Ramasamy SK, Kusumbe AP, Schiller M, Zeuschner D, Bixel MG, Milia C, Gamrekelashvili J, Limbourg A, Medvinsky A, Santoro MM, Limbourg FP, Adams RH. Blood flow controls bone vascular function and osteogenesis. Nat Commun. 2016;7(1):13601.

73. Azeem A, English A, Kumar P, Satyam A, Biggs M, Jones E, Tripathi B, Basu N, Henkel J, Vaquette C, Rooney N, Riley G, O'Riordan A, Cross G, Ivanovski S, Hutmacher D, Pandit A, Zeugolis D. The influence of anisotropic nano- to micro-topography on in vitro and in vivo osteogenesis. Nanomedicine-uk. 2015;10(5):693–711.

74. Mehdizadeh H, Sumo S, Bayrak ES, Brey EM, Cinar A. Three-dimensional modeling of angiogenesis in porous biomaterial scaffolds. Biomaterials. 2013;34(12):2875–87.

75. Hsieh Y-F, Robling AG, Ambrosius WT, Burr DB, Turner CH. Mechanical Loading of Diaphyseal Bone In Vivo: The Strain Threshold for an Osteogenic Response Varies with Location. J Bone Miner Res. 2001;16(12):2291–7.

76. Mapara M, Thomas BS, Bhat K. Rabbit as an animal model for experimental research. Dent Res J. 2012;9(1):111.

77. Schmitz JP, Hollinger JO. The Critical Size Defect as an Experimental Model for Craniomandibulofacial Nonunions. Clin Orthop Relat R. 1986;NA;(205):299???308.

78. Schemitsch EH. Size Matters: Defining Critical in Bone Defect Size. J Orthop Trauma. 2017;31(NA;):S20–2.

79. F04 AC. Guide for Pre-clinical in vivo Evaluation in Critical Size Segmental Bone Defects. 2014;

80. Pearce A, Richards R, Milz S, Schneider E, Pearce S. Animal models for implant biomaterial research in bone: A review. European Cells Mater. 2007;13:1–10.

81. Li Y, Chen S-K, Li L, Qin L, Wang X-L, Lai Y-X. Bone defect animal models for testing efficacy of bone substitute biomaterials. J Orthop Transl. 2015;3(3):95–104.

82. Clarke B. Normal Bone Anatomy and Physiology. Clin J Am Soc Nephro. 2008;3(Supplement 3):S131–9.

83. Magal RA, Reznikov N, Shahar R, Weiner S. Three-dimensional structure of minipig fibrolamellar bone: Adaptation to axial loading. J Struct Biol. 2014;186(2):253–64.

84. Barrera JW, Cabec AL, Barak MM. The orthotropic elastic properties of fibrolamellar bone tissue in juvenile white-tailed deer femora. J Anat. 2016;229(4):568–76.

85. Weiner S, Traub W, Wagner HD. Lamellar Bone: Structure–Function Relations. J Struct Biol. 1999;126(3):241–55.

86. Turner CH, Forwood MR, Rho J-Y, Yoshikawa T. Mechanical loading thresholds for lamellar and woven bone formation. J Bone Miner Res. 2009;9(1):87–97.

87. Marsell R, Einhorn TA. The biology of fracture healing. Inj. 2011;42(6):551–5.

88. AI-Aql ZS, Alagl AS, Graves DT, Gerstenfeld LC, Einhorn TA. Molecular Mechanisms Controlling Bone Formation during Fracture Healing and Distraction Osteogenesis. J Dent Res. 2008;87(2):107–18.

89. Corradetti B. The Immune Response to Implanted Materials and Devices. 2017;

90. Tonnesen MG, Feng X, Clark RAF. Angiogenesis in Wound Healing. J Invest Derm Symp P. 2000;5(1):40–6.

91. Esposito M, Hirsch J, Lekholm U, Thomsen P. Biological factors contributing to failures of osseointegrated oral implants, (I). Success criteria and epidemiology. Eur J Oral Sci. 1998;106(1):527–51.

92. Davies JE. Mechanisms of endosseous integration. Int J Prosthodont. 1998;11(5):391–401.

93. Anderson JM. Inflammatory Response to Implants. Asaio J. 1988;34(2):101–7.

94. Taniguchi N, Fujibayashi S, Takemoto M, Sasaki K, Otsuki B, Nakamura T, Matsushita T, Kokubo T, Matsuda S. Effect of pore size on bone ingrowth into porous titanium implants fabricated by additive manufacturing: An in vivo experiment. Mater Sci Eng C. 2016;59:690–701.

95. Li G, Wang L, Pan W, Yang F, Jiang W, Wu X, Kong X, Dai K, Hao Y. In vitro and in vivo study of additive manufactured porous Ti6Al4V scaffolds for repairing bone defects. Sci Rep-uk. 2016;6(1):34072.

96. Bai F, Wang Z, Lu J, Liu J, Chen G, Lv R, Wang J, Lin K, Zhang J, Huang X. The Correlation Between the Internal Structure and Vascularization of Controllable Porous Bioceramic Materials In Vivo: A Quantitative Study. Tissue Eng Pt A. 2010;16(12):3791–803.

97. Ponader S, von Wilmowsky C, Widenmayer M, Lutz R, Heinl P, Körner C, Singer RF, Nkenke E, Neukam FW, Schlegel KA. In vivo performance of selective electron beam-melted Ti-6Al-4V structures. J Biomed Mater Res A. 2010;92A(1):56–62.

98. Carluccio D, Xu C, Venezuela J, Cao Y, Kent D, Bermingham M, Demir AG, Previtali B, Ye Q, Dargusch M. Additively manufactured iron-manganese for biodegradable porous load-bearing bone scaffold applications. Acta Biomater. 2020;103:346–60.

99. Claes LE, Heigele CA. Magnitudes of local stress and strain along bony surfaces predict the course and type of fracture healing. J Biomech. 1999;32(3):255–66.

100. Bosshardt DD, Chappuis V, Buser D. Osseointegration of titanium, titanium alloy and zirconia dental implants: current knowledge and open questions. Periodontol 2000. 2017;73(1):22–40.

101. Chang JZ-C, Tsai P-I, Kuo MY-P, Sun J-S, Chen S-Y, Shen H-H. Augmentation of DMLS Biomimetic Dental Implants with Weight-Bearing Strut to Balance of Biologic and Mechanical Demands: From Bench to Animal. Materials. 2019;12(1):164.

102. Itälä AI, Ylänen HO, Ekholm C, Karlsson KH, Aro HT. Pore diameter of more than 100 μm is not requisite for bone ingrowth in rabbits. J Biomed Mater Res. 2001;58(6):679–83.

103. Ilea A, Vrabie O-G, Băbțan A-M, Miclăuş V, Ruxanda F, Sárközi M, Barbu-Tudoran L, Mager V, Berce C, Boşca BA, Petrescu NB, Cadar O, Câmpian RS, Barabás R. Osseointegration of titanium scaffolds manufactured by selective laser melting in rabbit femur defect model. J Mater Sci Mater Medicine. 2019;30(2):26.

104. Reinwald S, Burr D. Review of Nonprimate, Large Animal Models for Osteoporosis Research. J Bone Miner Res. 2008;23(9):1353–68.

105. Faria PEP, Carvalho AL, Felipucci DNB, Wen C, Sennerby L, Salata LA. Bone Formation Following Implantation of Titanium Sponge Rods into Humeral Osteotomies in Dogs: A Histological and Histometrical Study. Clin Implant Dent R. 2010;12(1):72–9.

106. Recker RR, Kimmel DB, Dempster D, Weinstein RS, Wronski TJ, Burr DB. Issues in modern bone histomorphometry. Bone. 2011;49(5):955–64.

107. Seong W, Grami S, Jeong SC, Conrad HJ, Hodges JS. Comparison of Push-In versus Pull-Out Tests on Bone-Implant Interfaces of Rabbit Tibia Dental Implant Healing Model. Clin Implant Dent R. 2013;15(3):460–9.

108. Palmquist A, Snis A, Emanuelsson L, Browne M, Thomsen P. Long-term biocompatibility and osseointegration of electron beam melted, free-form–fabricated solid and porous titanium alloy: Experimental studies in sheep. J Biomater Appl. 2013;27(8):1003–16.

109. Liu F, Mao Z, Zhang P, Zhang DZ, Jiang J, Ma Z. Functionally graded porous scaffolds in multiple patterns: New design method, physical and mechanical properties. Mater Design. 2018;160(Biomaterials 23 2002):849–60.

110. Arabnejad S, Johnston RB, Pura JA, Singh B, Tanzer M, Pasini D. High-strength porous biomaterials for bone replacement: A strategy to assess the interplay between cell morphology, mechanical properties, bone ingrowth and manufacturing constraints. Acta Biomater. 2016;30:345–56.

111. Lee J, Cha HD, Shim J, Jung JW, Kim JY, Cho D. Effect of pore architecture and stacking direction on mechanical properties of solid freeform fabrication-based scaffold for bone tissue engineering. J Biomed Mater Res A. 2012;100A(7):1846–53.

112. de Wild M, Zimmermann S, Rüegg J, Schumacher R, Fleischmann T, Ghayor C, Weber FE. Influence of Microarchitecture on Osteoconduction and Mechanics of Porous Titanium Scaffolds Generated by Selective Laser Melting. 3d Print Addit Manuf. 2016;3(3):142–51.

113. de Wild M, Ghayor C, Zimmermann S, Rüegg J, Nicholls F, Schuler F, Chen T-H, Weber FE. Osteoconductive Lattice Microarchitecture for Optimized Bone Regeneration. 3d Print Addit Manuf. 2019;6(1):40–9.

114. Wang H, Su K, Su L, Liang P, Ji P, Wang C. The effect of 3D-printed Ti6Al4V scaffolds with various macropore structures on osteointegration and osteogenesis: A biomechanical evaluation. J Mech Behav Biomed. 2018;88(J. Mech. Behav. Biomed. Mater. 34 2014):488–96.

115. Ran Q, Yang W, Hu Y, Shen X, Yu Y, Xiang Y, Cai K. Osteogenesis of 3D printed porous Ti6Al4V implants with different pore sizes. J Mech Behav Biomed. 2018;84(Crit. Rev. Biomed. Eng. 40 2012):1–11.

116. Lopez-Heredia MA, Goyenvalle E, Aguado E, Pilet P, Leroux C, Dorget M, Weiss P, Layrolle P. Bone growth in rapid prototyped porous titanium implants. J Biomed Mater Res A. 2008;85A(3):664–73.

117. Schouman T, Schmitt M, Adam C, Dubois G, Rouch P. Influence of the overall stiffness of a load-bearing porous titanium implant on bone ingrowth in critical-size mandibular bone defects in sheep. J Mech Behav Biomed. 2016;59:484–96.

118. Wieding J, Lindner T, Bergschmidt P, Bader R. Biomechanical stability of novel mechanically adapted open-porous titanium scaffolds in metatarsal bone defects of sheep. Biomaterials. 2015;46:35–47.

119. Bobyn JD, Pilliar RM, Cameron HU, Weatherly GC. The optimum pore size for the fixation of porous-surfaced metal implants by the ingrowth of bone. Clin Orthop Relat R. 1980;NA;(150):263–70.

120. Bandyopadhyay A, Mitra I, Shivaram A, Dasgupta N, Bose S. Direct comparison of additively manufactured porous Titanium and Tantalum implants towards in vivo osseointegration. Addit Manuf. 2019;28:259–66.

121. Xiu P, Jia Z, Lv J, Yin C, Cheng Y, Zhang K, Song C, Leng H, Zheng Y, Cai H, Liu Z. Tailored Surface Treatment of 3D Printed Porous Ti6Al4V by Microarc Oxidation for Enhanced Osseointegration via Optimized Bone In-Growth Patterns and Interlocked Bone/Implant Interface. Acs Appl Mater Inter. 2016;8(28):17964–75.

122. Deering J, Clifford A, D'Elia A, Zhitomirsky I, Grandfield K. Composite Dip Coating Improves Biocompatibility of Porous Metallic Scaffolds. Mater Lett. 2020;274:128057.

123. Liu X, Chu PK, Ding C. Surface modification of titanium, titanium alloys, and related materials for biomedical applications. Mater Sci Eng R Reports. 2004;47(3–4):49–121.

124. Wang J, Tang J, Zhang P, Li Y, Wang J, Lai Y, Qin L. Surface modification of magnesium alloys developed for bioabsorbable orthopedic implants: A general review. J Biomed Mater Res Part B Appl Biomaterials. 2012;100B(6):1691–701.

125. Asri RIM, Harun WSW, Samykano M, Lah NAC, Ghani SAC, Tarlochan F, Raza MR. Corrosion and surface modification on biocompatible metals: A review. Mater Sci Eng C. 2017;77:1261–74.

126. Chouirfa H, Bouloussa H, Migonney V, Falentin-Daudré C. Review of titanium surface modification techniques and coatings for antibacterial applications. Acta Biomater. 2018;83:37–54.